# Programmable Triangulation Light Curtains

Jian Wang, Joseph Bartels, William Whittaker,
Aswin C. Sankaranarayanan, and Srinivasa G. Narasimhan

Carnegie Mellon University, Pittsburgh PA 15213, USA
{jianwan2,josephba,saswin}@andrew.cmu.edu,
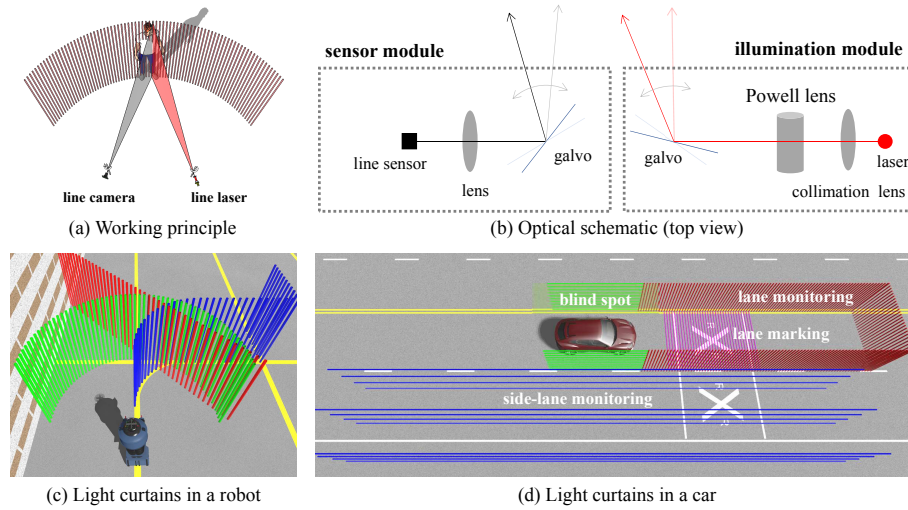{red}@cmu.edu, {srinivas}@cs.cmu.edu

**Abstract.** A vehicle on a road or a robot in the field does not need a full-featured 3D depth sensor to detect potential collisions or monitor its blind spot. Instead, it needs to only monitor if any object comes within its near proximity which is an easier task than full depth scanning. We introduce a novel device that monitors the presence of objects on a virtual shell near the device, which we refer to as a light curtain. Light curtains offer a light-weight, resource-efficient and programmable approach to proximity awareness for obstacle avoidance and navigation. They also have additional benefits in terms of improving visibility in fog as well as flexibility in handling light fall-off. Our prototype for generating light curtains works by rapidly rotating a line sensor and a line laser, in synchrony. The device is capable of generating light curtains of various shapes with a range of 20-30m in sunlight (40m under cloudy skies and 50m indoors) and adapts dynamically to the demands of the task. We analyze properties of light curtains and various approaches to optimize their thickness as well as power requirements. We showcase the potential of light curtains using a range of real-world scenarios.

**Keywords:** Computational imaging · Proximity sensors

## 1 Introduction

3D sensors play an important role in the deployment of many autonomous systems including field robots and self-driving cars. However, there are many tasks for which a full-fledged 3D scanner is often unnecessary. For example, consider a robot that is maneuvering a dynamic terrain; here, while full 3D perception is important for long-term path planning, it is less useful for time-critical tasks like obstacle detection and avoidance. Similarly, in autonomous driving, collision avoidance — a task that must be continually performed — does not require full 3D perception of the scene. For such tasks, a proximity sensor with much reduced energy and computational footprint is sufficient.

We generalize the notion of proximity sensing by proposing an optical system to detect the presence of objects that intersect a virtual shell around the system. By detecting only the objects that intersect with the virtual shell, we can solve many tasks pertaining to collision avoidance and situational awareness with little or no computational overhead. We refer to this virtual shell as a *light curtain*.

(a) Working principle

(b) Optical schematic (top view)

(c) Light curtains in a robot

(d) Light curtains in a car

**Fig. 1.** We introduce the concept of a programmable triangulation light curtain — a safety device that monitors object presence in a virtual shell around the device. (a, b) This is implemented by intersecting a light plane emitted from a line laser and a plane imaged by a line scan camera. The two planes are rapidly rotated in synchrony to generate light curtains of varying shapes as demanded by the specifics of an application. (c, d) Example curtains are shown for use on a robot and a car. The device detects objects on the virtual curtains with little computational overhead, making it useful for collision detection and avoidance.

We implement light curtains by triangulating an illumination plane, created by fanning out a laser, with a sensing plane of a line sensor (see Fig. 1(a)). In the absence of ambient illumination, the camera senses light only from the intersection between these two planes — which is a line in the physical world. The light curtain is then created by sweeping the illumination and sensing planes in synchrony. This idea can be interpreted as a generalization of pushbroom stereo [6] to active illumination for determining the presence of an object that intersects an arbitrary ruled surface in 3D.

**Benefits of triangulation light curtains.** (1) *Shape programmability*: The shape of a light curtain is programmable and can be configured dynamically to suit the demands of the immediate task. For example, light curtains can be used to determine whether a neighboring vehicle is changing lanes, whether a pedestrian is in the crosswalk, or whether there are vehicles in adjacent lanes. Similarly, a robot might use a curtain that extrudes its planned (even curved) motion trajectory. Fig. 1(c, d) shows various light curtains for use in robots and cars.

(2) *Adaptability of power and exposure*: Given an energy budget, in terms of average laser power, exposure time, and refresh rate of the light curtain, we can allocate higher power and exposure to lines in the curtain that are further away

to combat inverse-square light fall-off. This is a significant advantage over traditional depth sensors that typically expend the same high power in all directions to capture a 3D point cloud of the entire volume.

(3) *Performance in scattering media*: The optical design of the light curtain shares similarities with confocal imaging [16] in that we selectively illuminate and sense a small region. When imaging in scattering media, such as fog and murky waters, this has the implicit advantage that back scattered photons are optically avoided, thereby providing images with increased contrast.

(4) *Performance in ambient light*: A key advantage of programmable light curtains is that we can concentrate the illumination and sensing to a thin region. Together with the power and exposure adaptability, this enables significantly better performance under strong ambient illumination, including direct sunlight, at large distances ($\sim$20-30$m$). The performance increases under cloudy skies and indoors to 40$m$ and 50$m$ respectively.

(5) *Dynamic range of the sensor*: At any time instant, the sensor only captures a single line of the light curtain that often has small depth variations and consequently, little variation in intensity fall-off. Thus, the dynamic range of the measured brightness is often low. Hence, even a one-bit sensor with a programmable threshold would be ample for the envisioned tasks.

(6) *Sensor types*: Any line sensor could be used with our design including intensity sensors (CMOS, CCD, InGaAs [12]), time-of-flight (ToF) sensors (correlation, SPAD [8]), and neuromorphic sensors (DVS) [15].

**Limitations of triangulation light curtains.** (1) *Line-of-sight to the light curtain.* Our technique requires that the laser and sensor have line-of-sight to the light curtain. When this is not the case, the intersection of line camera plane and laser sheet is inside the object and is not seen by the camera; so the technique will fail to detect objects intersecting with the light curtain. This can be resolved partially by determining if there is an object between the system and the desired curtain using a curtain whose "shape" is a sparse set of lines. (2) *Interference*: When simultaneously used, several devices can accidentally interfere with each other. This can be alleviated by using a time-of-flight sensor with different light amplitude frequencies or adding a second line camera or several line lasers as further discussed in the supplementary material. (3) *Fast motion*: Objects that move at high speeds might be able to avoid detection by crossing the light curtain in a region between two successive scans. However, the target would need to be highly maneuverable to accomplish this given our high scan rate.

## 2   Related Work

*Safety devices and proximity sensors.* Devices such as "light curtains" [1], pressure-sensitive mats, and conductive rubber edges are common safeguards used in homes and factories. They are designed to stop the operation of a machine (e.g. a garage door) automatically upon detection of a nearby object. Such proximity sensing devices use many physical modalities to detect presence including capacitance, inductance, magnetism, infrared, ultrasound, Radar and LIDAR.

*Depth gating.* Temporal gating [5, 10] uses a combination of a pulsed laser and a camera with gated shutter, typically in the range of pico- to nano-seconds. By delaying the exposure of the camera with respect to the laser pulse, the device enables depth selection. An alternate approach relies on on-chip implementations of temporal modulated light sources and sensors [22]. Our technique can be interpreted as a specialized instance of primal-dual coding [20] where simultaneous coding is performed at the camera and projector to probe the light transport matrix associated with a scene, including implementing depth gating.

The proposed technique is inspired from existing work on robust depth scanning in presence of global and ambient light. Early work on imaging through turbid includes scanning confocal microscopy [16] and light sheet microscopy [25] which both illuminate and image the same depth with very shallow depth of focus and block out-of-focus light i.e. scattered light during image formation. Recent work for 3D measuring in scattering media have line striping-based [18] and SPAD-based [21] methods through analyzing spatial or temporal distribution of photons, respectively. An effective method for handling ambient light is concentrating the active light source's output and scanning. Gupta et al. [11] adjust the light concentration level in a structured light system adaptively according to the ambient light level. Episcan3D [19] and EpiToF [3] scan a line laser and a line sensor in synchrony such that the illumination and the sensing planes are coplanar. Finally, there are many benefits in using special functionality sensors for imaging and depth scanning; examples include the DVS sensor for structured light point scanning at high speed and dynamic range [17] as well as the short-wave infrared sensor for enhanced eye-safe property and decreased scattering [26, 24]. Such sensors can be easily incorporated in our light curtains for additional robustness and capabilities.

## 3   Geometry of Triangulation Light Curtains

The proposed device consists of a line scan camera and a line scan laser, as shown in Fig. 1(a, b). A Powell lens fans a laser beam out into a planar sheet of light and the line camera senses light from a single plane. In the general configuration, the two planes intersect at a line in 3D and, in the absence of ambient and indirect illuminations, the sensor measures light scattered by any object on the line. By rotating both the camera and the laser at a high speed, we can sweep the intersecting line to form any ruled surface [2]. We refer to this ruled surface, on which we detect presence of objects, as the light curtain. The resulting device is programmable, in terms of its light curtain shape, and flexible, in terms of being able to vary laser power and camera exposure time to suit the demands of an application. In this section, we present the mathematical model for a light curtain as a function of the camera and laser rotation axes. Then, we describe how to estimate the camera and laser rotation angles for a particular light curtain shape and show several examples.

We consider the case where the camera and laser can each be rotated about a single fixed parallel axis (see Fig. 2). This can be easily implemented by placing

(a) Parallel rotation axis      (b) Coordinate system      (c) Top view
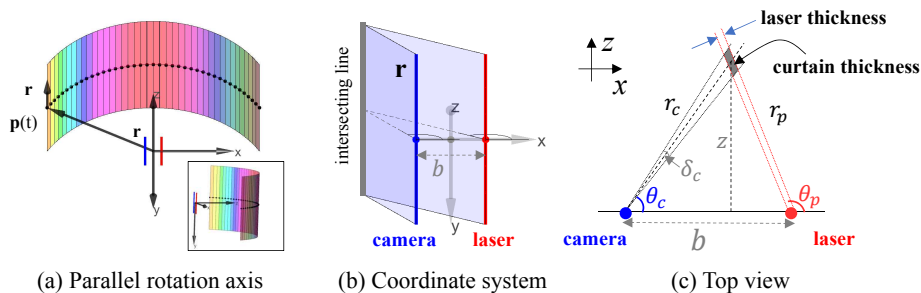
**Fig. 2.** (a) Viewing and illumination geometry of a triangulation light curtain generated by rotating the laser light plane and sensor plane about parallel axes **r**. The intersection line is also parallel to the two rotation axes. (b, c) The coordinate frame and top view showing various parameters of interest. Note that changing $\theta_c$ and $\theta_p$ in synchrony generates light curtains with different shapes. (c) The finite sizes of camera pixels and finite thickness of laser sheet leads to a thick light curtain upon triangulation.

two 1D galvo mirrors, one each in the front of the line sensor and the laser, respectively. Let the camera and laser rotation axes be **r**. We observe that intersecting line in the curtain will also be parallel and of the form

$$\mathbf{p}_0 + u\mathbf{r},$$

where $\mathbf{p}_0$ is any 3D point on the line and $u \in (-\alpha, \alpha)$ is the offset along the axis of rotation (see Fig. 2(a, b)). Then, the light curtain $s(t, u) \subset \mathbb{R}^3$ is obtained by sweeping the intersection line such that
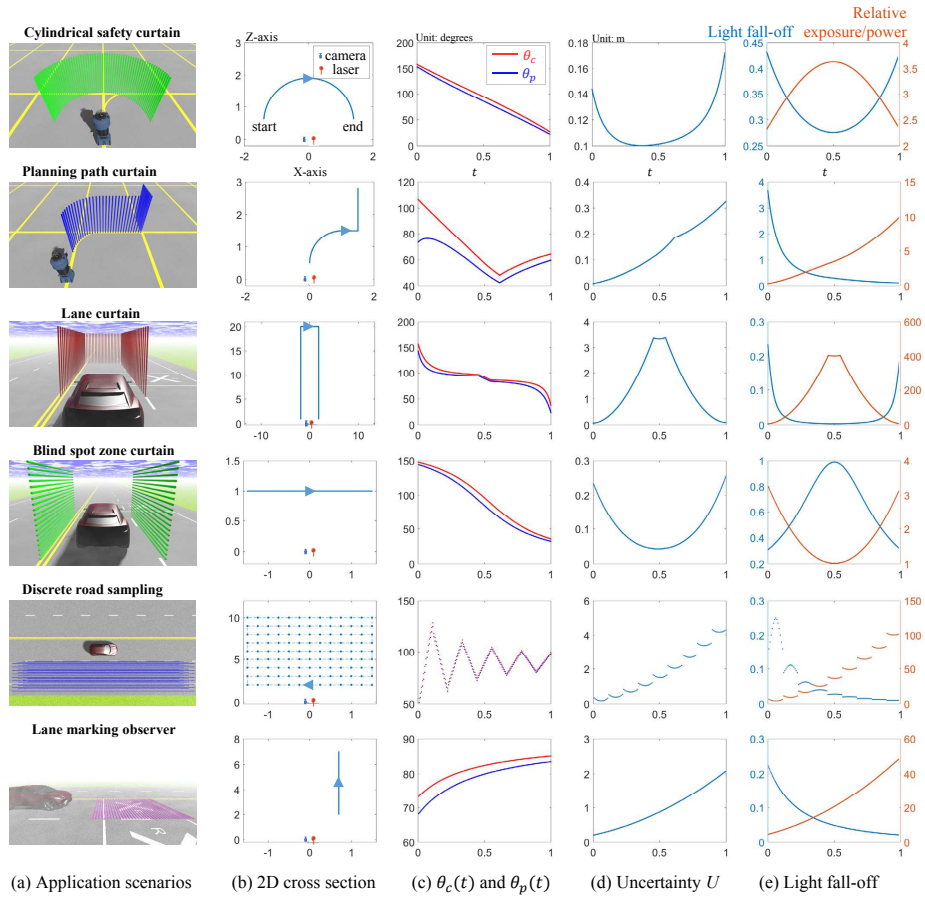
$$s(t, u) = \mathbf{p}(t) + u\mathbf{r},$$

where $\mathbf{p}(t) \in \mathbb{R}^3$ is a 3D path that describes the points scanned by the center pixel on the line sensor and $t \in [0, 1]$ is the parameterization of the path.

Given a light curtain $s(t, u)$, we next show how to compute the rotation angles of the camera and laser respectively. Without loss of generality, we assume that the origin of our coordinate system is at the midpoint between the centers of the line camera and the laser. We further assume that the rotation axes are aligned along the y-axis and that the 3D path can be written as $\mathbf{p}(t) = [x(t), 0, z(t)]^\top$. To achieve this light curtain, suppose that the laser rotates about its axis with an angular profile of $\theta_p(t)$, where the angle is measured counter-clockwise with respect to the x-axis. Similarly, the line sensor rotates with an angular profile of $\theta_c(t)$. Let $b$ be the baseline between the laser and the line camera. We can derive $\theta_c(t)$ and $\theta_p(t)$ as

$$\begin{bmatrix} \theta_c(t) \\ \theta_p(t) \end{bmatrix} = \begin{bmatrix} \text{atan2}(z(t), x(t) + b/2) \\ \text{atan2}(z(t), x(t) - b/2) \end{bmatrix}. \tag{1}$$

Fig. 1(c, d) shows different types of light curtains for use on robots and cars and Fig. 3 explains each in detail. For each curtain, we show the rendered scene

| Cylindrical safety curtain | | | | |
| Planning path curtain | | | | |
| Lane curtain | | | | |
| Blind spot zone curtain | | | | |
| Discrete road sampling | | | | |
| Lane marking observer | | | | |
| (a) Application scenarios | (b) 2D cross section | (c) $\theta_c(t)$ and $\theta_p(t)$ | (d) Uncertainty $U$ | (e) Light fall-off |

**Fig. 3.** Different types of light curtains used by a robot and a car. (a) Envisioned application scenarios visualized using 3D renderings. (b) 2D cross section (all units in meters) of the light curtain and placement of the camera and laser (baselines in the first two rows was 300mm, third row was 2m, and the remaining rows was 200mm). The arrow on the curtain indicates the scanning direction. (c) Rotation angle profiles of camera and laser to achieve desired light curtain in each scan. (d) Thickness of the light curtain for a camera with $50\mu m$ pixel width and focal length 6mm. (e) Light fall-off and the corresponding adaptation of exposure/power to compensate for it.

with the light curtain, a 2D cross section of the curtain, and the corresponding rotation angle profiles $\theta_c(t)$ and $\theta_p(t)$, computed using (1). The first two light curtains — a cylindrical curtain for safety zone monitoring and a curved curtain for monitoring obstacles along a path — are envisioned for use on robots. The next four kinds of curtains are envisioned for use on cars: ⊓-shape lane curtain to detect proximity vehicles in front as well as those that encroach on to the lane being used (row 3), side curtain to cover blind spot zones (row 4), and a discrete

sampling of neighbor lane's condition to identify presence of a vehicle in that volume (row 5). As noted in the introduction, light curtains also offer improved contrast in the presence of scattering media and hence, a curtain observing lane markings (row 6) is especially useful on foggy days.

Our proposed device can also be configured with the line sensor and laser rotating over non-parallel axes or even with each of them enjoying full rotational degree of freedom. These configurations can generate other kinds of ruled surfaces including, for example, a Möbius strip. We leave the discussion to the supplementary material. For applications that require light curtains of arbitrary shapes, we would need to use point sources and detectors; this, however, comes at the cost of large acquisition time that is required for two degrees of freedom in scanning. On the other hand, 2D imaging with a divergent source does not require any scanning but has poor energy efficiency and flexibility. In comparison, line sensors and line lasers provide a unique operating point with high acquisition speeds, high energy efficiency, and a wide range of light curtain shapes.

## 4  Optimizing Triangulation Light Curtains

We now quantify parameters of interest in practical light curtains — for example their thickness and signal-to-noise ratio (SNR) of measured detections — and approaches to optimize them. In particular, we are interested in minimizing thickness of the curtain as well as optimizing exposure time and laser power for improved detection accuracy when the curtain spans a large range of depths.

*Thickness of light curtain.* The light curtain produced by our device has a finite thickness due to the finite sizes of the sensor pixels and the laser illumination. Suppose that the laser plane has a thickness of $\Delta_L$ meters and each pixel has an angular extent of $\delta_c$ radians. Given a device with a baseline of length $b$ meters and imaging a point at depth $z(t) = z$, the thickness of the light curtain is given as an area of a parallelogram shaded in Fig. 2(c), which evaluates to

$$A = \frac{r_c^2 r_p}{z} \frac{\delta_c \Delta_L}{b} \tag{2}$$

where $r_c$ and $r_p$ is the distance between the intersected point and the camera and laser, respectively. We provide the derivation in the supplemental material. Finally, given that different light curtain geometries can produce curtains of the same area, a more intuitive and meaningful metric for characterizing the thickness is the length

$$U = \frac{A}{\Delta_L} = \frac{r_c^2 r_p}{z} \frac{\delta_c}{b}. \tag{3}$$

In any given system, changing the laser thickness $\Delta_L$ requires changing the optics of the illumination module. Similarly, changing $\delta_c$ requires either changing the pixel width or the focal length of the camera. In contrast, varying the baseline provides an easier alternative to changing the thickness of the curtain that involves a single translation. This is important since different applications

often have differing needs on the thickness of the curtain. A larger baseline helps in achieving very thin curtains which is important when there is a critical need to avoid false alarm. On the other hand, thick curtains that can be achieved by having a smaller baseline are important in scenarios where mis-detections, especially those arising from the discreteness of the curtain, are to be avoided.

In Fig. 3(d), we visualize the thickness of various light curtains. We set the camera's pixel width to $50\mu$m with a lens of focal length $f = 6$mm, thereby giving us a value for $\delta_c = \frac{50\mu m}{f} = 0.008$ radians. The baseline $b$ was set to $300mm$ for the first two rows, $2m$ for the third row, and $200mm$ for the last three rows. For example, for the lane marking observer (last row), a thickness of $2m$ at the furthest point is beneficial to deal with uneven roads.

*Adapting laser power and exposure.* Another key advantage of our light curtain device is that we can adapt the power of the laser or the exposure time for each intersecting line to compensate for light fall-off, which is inversely proportional to the square of the depth. In a traditional projector-camera system, it is common to increase the brightness of the projection to compensate for light fall-off, so that far-away scenes points can be well illuminated; however, this would imply that points close to the camera get saturated easily thereby requiring a high dynamic range camera. In contrast, our system has an additional degree of freedom where-in the laser's power and/or the camera's exposure time can be adjusted according to depth so that light fall-off is compensated to the extent possible under the device constraints and eye safety. Further, because our device only detects presence or absence of objects, in an ideal scenario where albedo is the same everywhere, the laser can send small amounts of light to just overcome the camera's readout noise or the photon noise of ambient light, and only a 1-bit camera is required. Fig. 3(e) shows light fall-off and depth-adaptive exposure time or laser power for all the light curtains.

*Combining with time-of-flight sensors.* The analysis in (3) indicates that $U \approx \frac{z^2 \delta_c}{b}$ when $r_c, r_p \approx z$ and light curtain is expected to get thicker, quadratically, with depth. Increasing baseline and other parameters of the system can only alleviate this effect in part due to the physical constraints on sensor size, laser spot thickness as well as the baseline. We show that replacing the line intensity sensor with a 1D continuous-wave time-of-flight (CW-TOF) sensor [14] alleviates the quadratic dependence of thickness with depth.

CW-TOF sensors measure phase to obtain depth. A CW-TOF sensor works by illuminating the scene with an amplitude modulated wave, typically a periodic signal of frequency $f_m$ Hz, and measuring the phase difference between the illumination and the light received at each pixel. The phase difference $\phi$ and the depth $d$ of the scene point are related as

$$\phi = \mathrm{mod}\left(f_m d/c, 2\pi\right).$$

As a consequence, the depth resolution of a TOF sensor $\Delta d = \frac{c\Delta\phi}{f_m}$ (ignoring the phase wrapping) is constant and independent of depth. Further, the depth

resolution increases with the frequency of the amplitude wave. However, TOF-based depth recovery has a phase wrapping problem due to the presence of the $\mathrm{mod}(\cdot)$ operator; this implies that the depth estimate has an ambiguity problem and this problem gets worse at higher frequencies. In contrast, traditional triangulation-based depth estimation has no ambiguity problem, but at the cost of quadratic depth uncertainty.
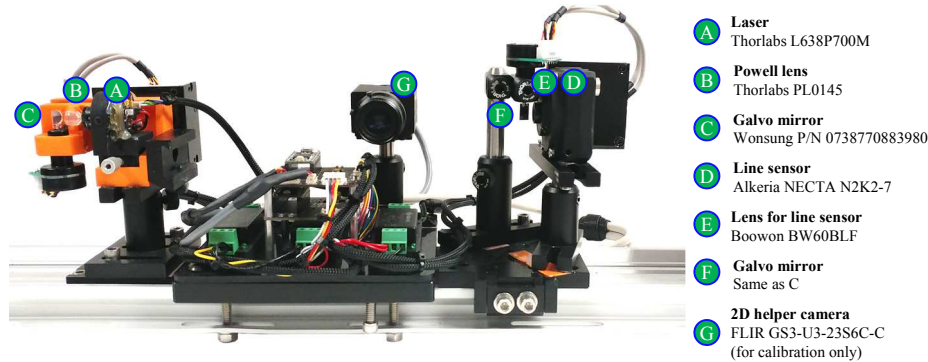
We can leverage the complementary strengths of traditional triangulation and CW-TOF to enable light curtains with near-constant thickness over a large range. This is achieved as follows. First, the phase and intensity of the triangulated region are measured by the CW-TOF sensor; examples of this is shown in Fig. 8(iii, iv). Second, knowing the depth of the curtain, we can calculate the appropriate phase to retain and discard pixels with phase values that are significantly different. An alternative approach to achieving this is to perform phase-based depth gating using appropriate codes at illumination and sensing [22]. The use of triangulation automatically eliminates the depth ambiguity of phase-based gating *provided* the thickness of the triangulation is smaller than half of the wavelength of the amplitude wave. With this, it is possible to create thinner light curtains over a larger depth range.

## 5   Hardware Prototype

Our prototype device has two modules (see Fig. 4). At the sensor end, we use an Alkeria NECTA N2K2-7 line intensity sensor with a 6mm $f/2$ S-mount lens whose diagonal FOV is 45° and image circle has a diameter of 7mm. The line camera has $2048 \times 2$ pixels with pixel size $7\mu m \times 7\mu m$; we only use the central $1000 \times 2$ pixels due to the lens' limited circle of illumination. The line sensor is capable of reading out $95,057$ lines/second. We fit it with an optical bandpass filter, $630nm$ center wavelength and $50nm$ bandwidth to suppress ambient light. For the ToF prototype, we used a Hamamatsu S11961-01CR sensor in place of the intensity sensor whose pixel size is $20\mu m \times 50\mu m$. We used a low cost 1D galvo mirror to rotate the camera's viewing angle. The 2D helper FLIR camera (shown in the middle) is used for one-time calibration of the device and visualizing the light curtains in the scene of interest by projecting the curtain to its view.

At the illumination side, we used a Thorlabs L638P700M 638nm laser diode with peak power of $700mW$. The laser is collimated and then stretched into a line with a 45° Powell lens. As with the sensor side, we used a 1D galvo mirror to steer the laser sheet. The galvo mirror has dimension of $11mm \times 7mm$, and has 22.5° mechanical angle and can give the camera and laser 45° FOV since optical angle is twice the mechanical angle. It needs $500\mu s$ to rotate 0.2° optical angle. A micro-controller (Teensy 3.2) is used to synchronize the camera, the laser and the galvos. Finally, we aligned the rotation axes to be parallel and fixed the baseline as $300mm$. The FOV is approximately 45° × 45°.

*Ambient light.* The camera also measures the contribution from the ambient light illuminating the entire scene. To suppress this, we capture two images at

**A** Laser
Thorlabs L638P700M

**B** Powell lens
Thorlabs PL0145

**C** Galvo mirror
Wonsung P/N 0738770883980

**D** Line sensor
Alkeria NECTA N2K2-7

**E** Lens for line sensor
Boowon BW60BLF

**F** Galvo mirror
Same as C

**G** 2D helper camera
FLIR GS3-U3-23S6C-C
(for calibration only)

**Fig. 4.** Hardware prototype with components marked. The prototype implements the schematic shown in Fig. 1(b).

each setting of the galvos — one with and one without the laser illumination, each with exposure of $100\mu s$. Subtracting the two suppresses the ambient image.

*Scan rate.* Our prototype is implemented with galvo mirrors that take about $500$ $\mu s$ to stabilize, which limits the overall frame-rate of the device. Adding two $100\mu s$ exposures for laser on and off, respectively, allows us to display 1400 lines per second. In our experiments, we design the curtains with 200 lines, and we sweep the entire curtain at a refresh rate of 5.6 fps. To increase the refresh rate, we can use higher-quality galvo mirrors with lower settling time, a 2D rolling shutter camera as in [19] or spatially-multiplexed line camera by digital micromirror device (DMD) [23] in the imaging side and a MEMS mirror on the laser side so that 30 fps can be easily reached.

*Calibration and eye safety.* Successful and safe deployment of light curtains require precise calibration as well as specifications of laser eye safety. Calibration is done by identifying the plane in the real world associated with each setting of laser's galvo and the line associated with each pair of camera's galvo and camera's pixel. We use a helper camera and projector to perform calibration, following steps largely adapted from prior work in calibration [7, 13]. The supplemental material has detailed explanation for both calibration and laser eye safety calculations based on standards [4].
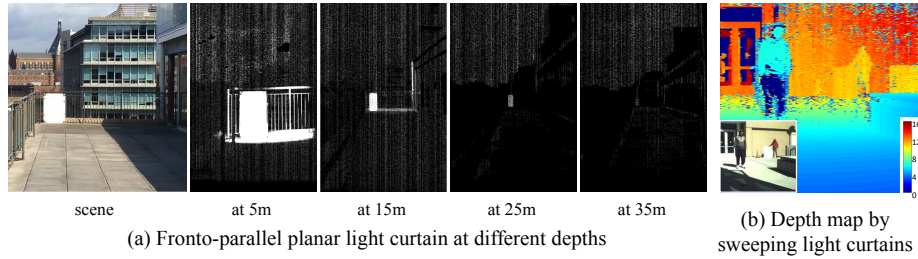
## 6   Results

*Evaluating programmability of triangulation light curtains.* Fig. 5 shows the results of implementing various light curtain shapes both indoors and outdoors. When nothing "touches" the light curtain, the image is dark; when a person or other intruders touch the light curtain, it is immediately detected. The small insets show the actual images captured by the line sensor (after ambient subtraction) mosaicked for visualization. The light curtain and the detection are
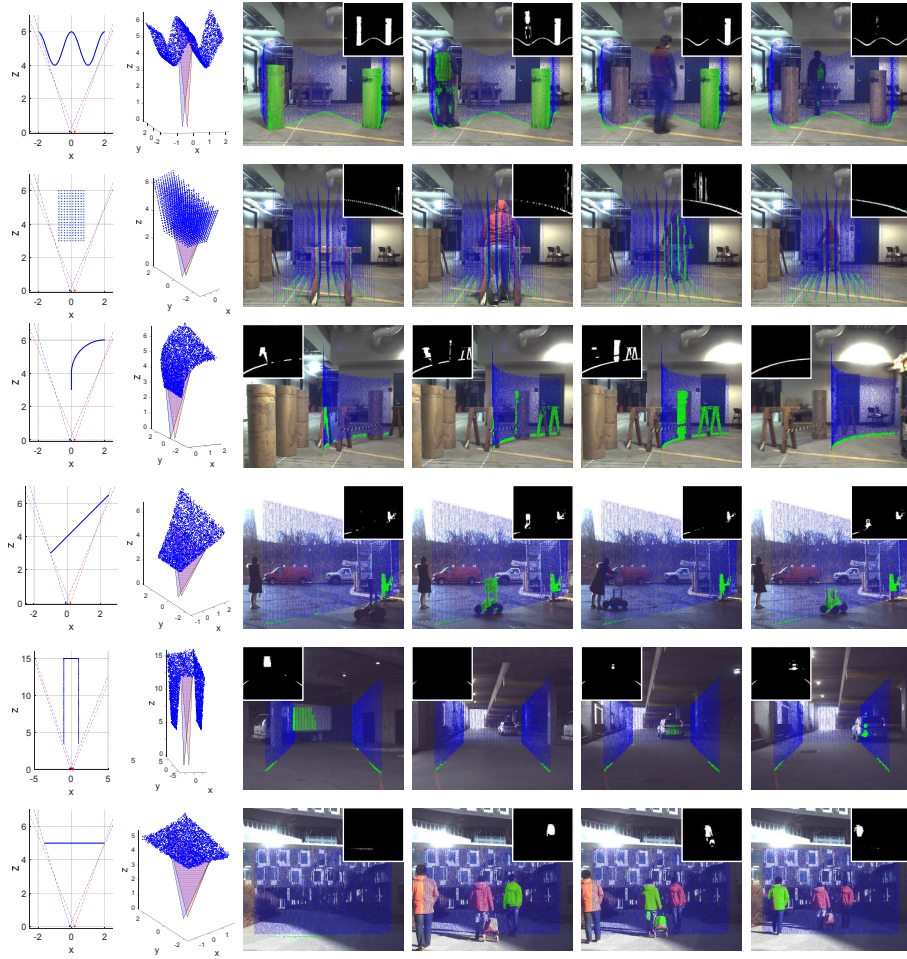
**Fig. 5.** Generating light curtains with different shapes. The images shown are from the 2D helper camera's view with the light curtain rendered in blue and detections rendered in green. The curtains are shown both indoors and outdoors in sunlight. The insets are images captured by the line sensor as people/objects intersect the curtains. The curtains have 200 lines with a refresh rate of 5.6 fps. The curtain in the second row detects objects by sampling a volume with a discrete set of lines.

geometrically mapped to the 2D helper camera's view for visualization. Our prototype uses a visible spectrum (red) laser and switching to near infrared can improve performance when the visible albedo is low (e.g. dark clothing).

*Light curtains under sunlight.* Fig. 6(a) shows the detections of a white board placed at different depths (verified using a laser range finder) in bright sunlight ($\sim 100klx$). The ambient light suppression is good even at 25m range. Under

|  | scene | at 5m | at 15m | at 25m | at 35m |
(a) Fronto-parallel planar light curtain at different depths

(b) Depth map by
sweeping light curtains

**Fig. 6.** Performance under bright sunlight (100*klux*) for two different scenes. (a) We show raw light curtain data, without post-processing, at various depths from a white board. Notice the small speck of the board visible even at 35m. (b) We sweep the light curtain over the entire scene to generate a depth map.
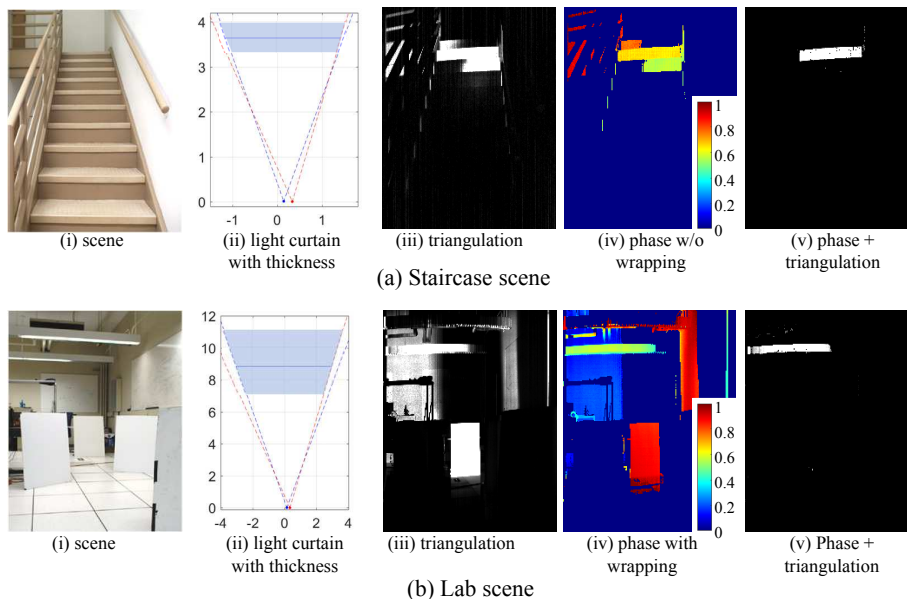


**Fig. 7.** Seeing through volumetric scattering media. Light curtains suppress backscattered light and provide images with improved contrast.

cloudy skies, the range increases to more than 40m. Indoors, the range is approximately 50m. These ranges assume the same refresh rate (and exposure time) for the curtains. In Fig. 6(b), we verify the accuracy of the planar curtains by sweeping a fronto-parallel curtain over a dense set of depths and visualizing the resulting detections as a depth map.

*Performance under volumetric scattering.* When imaging in scattering media, light curtains provide images with higher contrast by suppressing backscattered light from the medium. This can be observed in Fig. 7 where we show images of an outdoor road sign under heavy smoke from a planar light curtain as well as a conventional 2D camera. The 2D camera provides images with low contrast due to volumetric scattering of the sunlight, the ambient source in the scene.

*Reducing curtain thickness using a TOF sensor.* We use our device with a line TOF sensor to form a fronto-parallel light curtain at a fixed depth. The results are shown in Fig. 8. Because of triangulation uncertainty, the camera could see a wide depth range as shown in (a.iii) and (b.iii). However, phase data, (a.iv)

(i) scene    (ii) light curtain with thickness    (iii) triangulation    (iv) phase w/o wrapping    (v) phase + triangulation

(a) Staircase scene



(i) scene    (ii) light curtain with thickness    (iii) triangulation    (iv) phase with wrapping    (v) Phase + triangulation

(b) Lab scene

**Fig. 8.** Using line CW-TOF sensor. For both scenes, we show that fusing (iii) triangulation gating with (iv) phase information leads to (v) thinner light curtains without any phase wrapping ambiguity.

and (b.iv) helps to decrease the uncertainty as shown in (a.v) and (b.v). Note that in (b.iv), there is phase wrapping which is mitigated using triangulation.

*Adapting laser power and exposure.* Finally, we showcase the flexibility of our device in combating light fall-off by adapting the exposure and/or the power of the laser associated with each line in the curtain. We show this using depth maps sensed by sweeping fronto-parallel curtains with various depth settings. For each pixel we assign the depth value of the planar curtain at which its intensity value is the highest. We use an intensity map to save this highest intensity value. In Fig. 9(a), we sweep 120 depth planes in an indoor scene. We performed three strategies: two constant exposures per intersecting line and one that is depth-adaptive such that exposure is linear in depth. We show intensity map and depth map for each strategy. Notice the saturation and darkness in intensity maps with the constant exposure strategies and even brightness with the adaptive strategy. The performance of the depth-adaptive exposure is similar to that of a constant exposure mode whose total exposure time is twice as much. Fig. 9(b) shows a result on an outdoor scene with curtains at 40 depths, but here the power is adapted linearly with depth. As before, a depth-adaptive budgeting of laser power produces depth maps that are similar to those of a constant power mode with $2\times$ the total power. Strictly speaking, depth-adaptive budgeting should be quadratic though we use a linear approximation for ease of comparison.

(a) Constant exposure time vs. depth-adaptive exposure time



(b) Constant power vs. depth-adaptive power
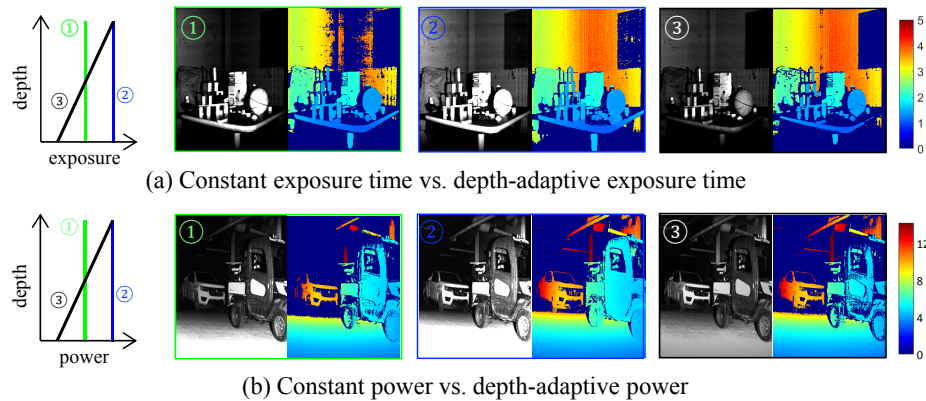
**Fig. 9.** We use depth adaptive budgeting of (a) exposure and (b) power to construct high-quality depth maps by sweeping a fronto-parallel curtain. In each case, we show the results of three strategies: (1) constant exposure/power at a low value, (2) constant exposure/power at a high value, and (3) depth-adaptive allocation of exposure/power such that the average matches the value used in (1). We observe that (3) achieves the same quality of depth map as (2), but using the same time/power budget as in (1).

## 7    Discussion

A 3D sensor like LIDAR is often used for road scene understanding today. Let us briefly see how it is used. The large captured point cloud is registered to a pre-built or accumulated 3D map with or without the help of GPS and IMU. Then, dynamic obstacles are detected, segmented, classified using complex, computationally heavy and memory intensive deep learning approaches [9, 27]. These approaches are proving to be more and more successful but perhaps all this computational machinery is not required to answer questions, such as: "Is an object cutting across into my lane?", or "Is an object in a cross-walk?".

This paper shows that our programmable triangulation light curtain can provide an alternative solution that needs little to no computational overhead, and yet has high energy efficiency and flexibility. We are by no means claiming that full 3D sensors are not useful but are asserting that light curtains are an effective addition when depths can be pre-specified. Given its inherent advantages, we believe that light curtains will be of immense use in autonomous cars, robotics safety applications and human-robot collaborative manufacturing.

## Acknowledgments

# References

1. Light curtain wikipedia. https://en.wikipedia.org/wiki/Light_curtain
2. Ruled surface wikipedia. https://en.wikipedia.org/wiki/Ruled_surface
3. Achar, S., Bartels, J.R., Whittaker, W.L., Kutulakos, K.N., Narasimhan, S.G.: Epipolar time-of-flight imaging. ACM Transactions on Graphics (TOG) **36**(4),  37 (2017)
4. American National Standards Institute: American national standard for safe use of lasers z136.1 (2014)
5. Baker, I.M., Duncan, S.S., Copley, J.W.: A low-noise laser-gated imaging system for long-range target identification. In: Defense and Security. pp. 133–144. International Society for Optics and Photonics (2004)
6. Barry, A.J., Tedrake, R.: Pushbroom stereo for high-speed navigation in cluttered environments. In: International Conference on Robotics and Automation (ICRA). pp. 3046–3052. IEEE (2015)
7. Bouguet, J.Y.: Matlab camera calibration toolbox. http://www.vision.caltech.edu/bouguetj/calib_doc/ (2000)
8. Burri, S., Homulle, H., Bruschini, C., Charbon, E.: Linospad: a time-resolved 256× 1 cmos spad line sensor system featuring 64 fpga-based tdc channels running at up to 8.5 giga-events per second. In: Optical Sensing and Detection IV. vol. 9899, p. 98990D. International Society for Optics and Photonics (2016)
9. Geiger, A., Lenz, P., Urtasun, R.: Are we ready for autonomous driving? the kitti vision benchmark suite. In: Conference on Computer Vision and Pattern Recognition (CVPR). pp. 3354–3361. IEEE (2012)
10. Grauer, Y., Sonn, E.: Active gated imaging for automotive safety applications. In: Video Surveillance and Transportation Imaging Applications 2015. vol. 9407, p. 94070F. International Society for Optics and Photonics (2015)
11. Gupta, M., Yin, Q., Nayar, S.K.: Structured light in sunlight. In: International Conference on Computer Vision (ICCV). pp. 545–552. IEEE (2013)
12. Hansen, M.P., Malchow, D.S.: Overview of swir detectors, cameras, and applications. In: Thermosense Xxx. vol. 6939, p. 69390I. International Society for Optics and Photonics (2008)
13. Lanman, D., Taubin, G.: Build your own 3d scanner: 3d photography for beginners. In: ACM SIGGRAPH 2009 Courses. p. 8. ACM (2009)
14. Li, L.: Time-of-flight camera–an introduction. Technical white paper (SLOA190B) (2014)
15. Lichtsteiner, P., Posch, C., Delbruck, T.: A 128x128 120 dB 15us latency asynchronous temporal contrast vision sensor. IEEE journal of solid state circuits **43**(2), 566–576 (2008)
16. Marvin, M.: Microscopy apparatus (Dec 19 1961), US Patent 3,013,467
17. Matsuda, N., Cossairt, O., Gupta, M.: Mc3d: Motion contrast 3d scanning. In: International Conference on Computational Photography (ICCP). pp. 1–10. IEEE (2015)
18. Narasimhan, S.G., Nayar, S.K., Sun, B., Koppal, S.J.: Structured light in scattering media. In: International Conference on Computer Vision (ICCV). vol. 1, pp. 420–427. IEEE (2005)
19. O'Toole, M., Achar, S., Narasimhan, S.G., Kutulakos, K.N.: Homogeneous codes for energy-efficient illumination and imaging. ACM Transactions on Graphics (ToG) **34**(4),  35 (2015)

20. O'Toole, M., Raskar, R., Kutulakos, K.N.: Primal-dual coding to probe light transport. ACM Transactions on Graphics (ToG) **31**(4), 39–1 (2012)
21. Satat, G., Tancik, M., Raskar, R.: Towards photography through realistic fog. In: International Conference on Computational Photography (ICCP). pp. 1–10. IEEE (2018)
22. Tadano, R., Kumar Pediredla, A., Veeraraghavan, A.: Depth selective camera: A direct, on-chip, programmable technique for depth selectivity in photography. In: International Conference on Computer Vision (ICCV). pp. 3595–3603. IEEE (2015)
23. Wang, J., Gupta, M., Sankaranarayanan, A.C.: Lisens-a scalable architecture for video compressive sensing. In: International Conference on Computational Photography (ICCP). IEEE (2015)
24. Wang, J., Sankaranarayanan, A.C., Gupta, M., Narasimhan, S.G.: Dual structured light 3d using a 1d sensor. In: European Conference on Computer Vision (ECCV). pp. 383–398. Springer (2016)
25. Weber, M., Mickoleit, M., Huisken, J.: Light sheet microscopy. In: Methods in cell biology, vol. 123, pp. 193–215. Elsevier (2014)
26. Wheaton, S., Bonakdar, A., Nia, I.H., Tan, C.L., Fathipour, V., Mohseni, H.: Open architecture time of fight 3d swir camera operating at 150 mhz modulation frequency. Optics Express **25**(16), 19291–19297 (2017)
27. Zhou, Y., Tuzel, O.: Voxelnet: End-to-end learning for point cloud based 3d object detection. Conference on Computer Vision and Pattern Recognition (CVPR) (2018)